Biochimica et Biophysica Acta 1838 (2014) 339–347

Contents lists available at ScienceDirect

Biochimica et Biophysica Acta

journal homepage: www.elsevier.com/locate/bbamem

Possible mechanism of structural transformations induced by *St*Asp-PSI in lipid membranes

Fernando Muñoz [a], M. Francisca Palomares-Jerez [b], Gustavo Daleo [a], José Villalaín [b,1], M. Gabriela Guevara [a,*,1]

[a] Plant Biochemistry Laboratory, Biological Research Institute, National Scientific and Technical Research Council, University of Mar del Plata, Mar del Plata 7600, Argentina
[b] Instituto de Biología Molecular y Celular, Universidad Miguel Hernández, E-03202 Elche, Alicante, Spain

ARTICLE INFO

Article history:
Received 21 February 2013
Received in revised form 2 August 2013
Accepted 6 August 2013
Available online 14 August 2013

Keywords:
Antimicrobial protein
Antitumor protein
Plant aspartic protease
Plant-specific insert
Membrane destabilization
α-Helix

ABSTRACT

In the present work we have analyzed the effect of *St*Asp-PSI (plant-specific insert of potato aspartic protease) on the structural and thermotropic properties of the major phospholipid types of bacterial and animal cells. Results obtained suggest that *St*Asp-PSI induces a destabilization of the membrane bilayers, depending on the time of interaction between the protein and the bilayers, rather than on its concentration. This temporal delay would be consistent with a lateral diffusion of *St*Asp-PSI monomers to assemble into aggregates to form pores. Like with the results previously reported for the *St*Asp-PSI circular dichroism, data obtained here from IR spectroscopy show that there are slight changes in the *St*Asp-PSI secondary structure in the presence of lipid membranes; suggesting that these changes could be related with the *St*Asp-PSI self-association. Results obtained from steady-state fluorescence anisotropy and differential scanning calorimetry assays suggest that *St*Asp-PSI interacts with both uncharged and negatively charged phospholipids, modulates the phase polymorphic behavior of model membranes and partitions and buries differentially in the membrane depending on the presence of negatively charged phospholipids.

1. Introduction

The clinical incidence of multi drug-resistant microbes has increased dramatically in recent decades [1,2]. Membrane-permeabilizing antimicrobial peptides (AMPs) have long been discussed as a possible novel class of antibiotics that could be used against multi drug-resistant microbes, but a poor understanding of the fundamental principles of AMP action has slowed the development of AMPs into clinical useful drugs [1].

AMPs are an integral part of the innate immune system of higher organisms [1,3–6]. These host defense proteins and peptides possess a wide spectrum of antimicrobial activity against eubacteria, fungi, viruses and eukaryotic parasites [2,7,8]. AMPs are attractive as therapeutic tools because they act without high specificity toward a protein target, which reduces the likelihood of induced resistance [9–11]. Therefore, understanding the mechanism of membrane permeabilization is crucial for the development of AMPs into useful antimicrobial agents [1].

Aspartic proteases (APs) (EC 3.4.23) are a class of widely distributed proteases present in animals, microbes, viruses and plants [12,13]. Biological functions of plant APs have not yet been characterized to the extent of their mammalian, microbial or viral counterparts [12–15]. Plant AP sequences predict preproproteins similar to the animal and fungal aspartic proteases, with a signal peptide and a proregion at the amino-terminus of the mature protein. Plant AP genes, with the exception of nucellin, a barley AP [16] and AP encoded by the *cdr*-1 gene from *Arabidopsis* [17], have an extra region of approximately 100 amino acids known as "plant specific insert" (PSI). This sequence has structural similarity with the precursor of mammalian saposins, lysosomal sphingolipid-activating proteins (SAPLIPs) [18,19].

Previously, we have reported the cloned, heterologous expression and purification of the PSI domain from a *Solanum tuberosum* aspartic protease (*St*Asp, accession number AY672651) named *St*Asp-PSI [20]. *St*Asp-PSI has high structural similarity with two lipid interacting proteins, saposin-*like* proteins (SAPLIPs), with antimicrobial activity NK-lysin and granulysin [20,21], both proteins classified as AMPs in the database available online at: http://aps.unmc.edu/AP/main.php [22]. Like these SAPLIPs, the *St*Asp-PSI domain is able to interact with cell plasma membranes, increasing the cell permeability and finally, producing cell death [20,23]. Additionally, we have demonstrated in previous reports that the cytotoxic activity of *St*APs and *St*Asp-PSI is selective [20,24]. Whereas these proteins are toxic to plant and human pathogenic microorganisms i.e., fungi, oomycetes, Gram − and Gram +

Abbreviations: AMPs, antimicrobial peptides and proteins; DMPC, 1,2-dimyristoylphosphatidylcholine; DMPG, 1,2-dimyristoylphosphatidylglycerol; DMPS, 1,2-dimyristoylphosphatidylserine; DPH, 1,6-diphenyl-1,3,5-hexatriene; DSC, differential scanning calorimetry; EPC, egg L-α-phosphatidylcholine; EPG, egg L-α-phosphatidylglycerol; IR, infrared spectroscopy; LUVs, large unilamellar vesicles; MLVs, multilamellar vesicles; PSI, plant-specific insert; SAPLIPs, saposin-like proteins; TMA-DPH, 1-(4-trimethylammoniumphenyl)-6-phenyl-1,3,5-hexatriene

* Corresponding author at: 3250 Funes, 4th Floor, Mar del Plata 7600, Argentina. Tel.: +54 223 4753030x14; fax: +54 223 4724143.
E-mail address: gguevara@mdp.edu.ar (M.G. Guevara).

[1] Equal contribution.

0005-2736/$ – see front matter © 2013 Elsevier B.V. All rights reserved.
http://dx.doi.org/10.1016/j.bbamem.2013.08.004

bacteria, as well as cancer cells, they are not able to kill human T cells, human red blood cells and plant cells [20,23–28]. Results obtained from vesicle leakage assays, circular dichroism spectroscopic measurements and analysis by size exclusion chromatography followed by electrophoresis showed that *St*Asp-PSI is a potent inducer of the leakage of LUVs composed of anionic phospholipids, especially those containing phosphatidylglycerol. Significantly, a hydrophobic environment is necessary for *St*Asp-PSI oligomerization and both *St*Asp-PSI disulfide bonds and negatively charged phospholipids are required to produce membrane destabilization which afterwards would induce cell death in tumors and microorganism cell targets. Moreover, the presence of cholesterol in the membrane strongly diminishes the capacity of *St*Asp-PSI to produce leakage, suggesting that the lack of hemolytic and cytotoxic activities on human lymphocytes of *St*Asp-PSI/*St*APs may be partly due to the presence of cholesterol in these types of cell membranes [29].

In order to deepen the mechanism of interaction between *St*Asp-PSI and phospholipid membranes, we have analyzed the structural changes in protein–membrane bilayer structures at the molecular level during their interaction. This study was performed using biophysical methods, namely measurements of leakage of a fluorescent probe, infrared spectroscopy (IR), steady-state fluorescence anisotropy and differential scanning calorimetry (DSC). The results obtained indicate that *St*Asp-PSI interacts with both uncharged and negatively charged phospholipids, modulates the phase polymorphic behavior of model membranes and partitions and buries differentially in the membrane depending on the presence of negatively charged phospholipids.

2. Materials and methods

2.1. Protein expression and purification

Recombinant *St*Asp-PSI was overexpressed in *Escherichia coli* M15 and purified as described previously [20]. Protein concentration was measured by the bicinchoninic acid method [30], using BSA as the standard.

2.2. Materials and reagents

Egg L-α-phosphatidylcholine (EPC), egg L-α-phosphatidylglycerol (EPG), 1,2-dimyristoylphosphatidylserine (DMPS), 1,2-dimyristoylphosphatidylcholine (DMPC), and 1,2-dimyristoylphosphatidylglycerol (DMPG) were obtained from Avanti Polar Lipids (Alabaster, AL, USA). Fluorescein isothiocyanate labeled dextran FD-70 and Triton X-100 were obtained from Sigma-Aldrich (Madrid, ES). 1,6-diphenyl-1,3,5-hexatriene (DPH), and 1-(4-trimethylammoniumphenyl)-6-phenyl-1,3,5-hexatriene (TMA-DPH) were obtained from Molecular Probes (Eugene, OR). All other chemicals were commercial samples of the highest purity available (Sigma-Aldrich, Madrid, ES). Water was deionized, twice-distilled and passed through a Milli-Q equipment (Millipore Ibérica, Madrid, ES) to a resistivity higher than 18 MΩ cm.

2.3. Vesicle preparation

Aliquots containing the appropriate amount of lipid in chloroform–methanol (2:1 vol/vol) were placed in a test tube, the solvents were removed by evaporation under a stream of O_2-free nitrogen, and finally, traces of solvents were eliminated under vacuum in the dark for more than 3 h. The lipid films were resuspended in an appropriate buffer and incubated either at 25 °C or 10 °C above the phase transition temperature (T_m) with intermittent vortexing for 30 min to hydrate the samples and obtain multilamellar vesicles (MLVs). The samples were frozen and thawed five times to ensure complete homogenization and maximization of peptide/lipid contacts with occasional vortexing. Large unilamellar vesicles (LUVs) with a mean diameter of 0.2 μm were prepared from MLVs by the extrusion method [31] using polycarbonate filters with a pore size of 0.2 μm (Nucleopore Corp., Cambridge, CA, USA). For infrared spectroscopy, aliquots containing the appropriate amount of lipid in chloroform/methanol (2:1 v/v) were dried by evaporation under a stream of O_2-free nitrogen and traces of solvents were eliminated under vacuum in the dark for more than 3. 300 μg of *St*Asp-PSI was placed in a test tube containing the dried lipid and then lyophilized (lipid/protein ratio 50:1). The samples were hydrated in 200 μl D_2O, mixed at 4 °C overnight, and lyophilized again. The samples were rehydrated in 30 μl D_2O and kept at 4 °C overnight to allow *St*Asp-PSI refolding. Finally, the suspensions were gently agitated at room temperature for 30 min to obtain MLVs and incubated at 40 °C for 1 h with occasional vortexing.

2.4. Membrane leakage measurement

For assays of vesicle leakage, LUVs with a mean diameter of 0.2 μm were prepared as indicated above in buffer containing 10 mM Tris–HCl, 100 mM NaCl, and 100 mg/ml FD70, pH 7.4. Non-encapsulated dextran was removed by gel-filtration chromatography using a pump P-50 (Amersham Pharmacia Biotech AB, Uppsala, Sweden) with a Sephacryl® 500-HR column eluted with the same buffer described above, at a flow rate of 3 ml/min. The final lipid concentration was 0.075 mM in a 5 mm × 5 mm fluorescence cuvette (final volume of 400 μl), stabilized at 25 °C and under constant stirring. Fluorescence was measured using a Varian Cary Eclipse spectrofluorimeter. One hundred percent release was achieved by adding Triton X-100 to either the microtiter plate or the cuvette to the final concentration of 0.5% (w/w). Changes in fluorescence intensity were recorded with excitation and emission wavelengths set at 492 and 517 nm, respectively. Excitation and emission slits were set at 5 nm. Leakage was quantified on a percentage basis as previously described by Bernabeu et al. and Moreno et al. [32,33].

2.5. Infrared spectroscopy

Approximately 30 μl of a resuspended sample in D_2O was placed between two CaF_2 windows separated by 50-μm thick Teflon spacers in a liquid demountable cell (Harrick, Ossining, NY). The spectra were obtained in a Bruker IFS55 spectrometer using a deuterated triglycine sulphate detector. Each spectrum was obtained by collecting 250 interferograms with a nominal resolution of 2 cm^{-1}, transformed using triangular apodization and, in order to average background spectra between sample spectra over the same time period, a sample shuttle accessory was used to obtain sample and background spectra. The spectrometer was continuously purged with dry air at a dew point of −40 °C in order to remove atmospheric water vapor from the bands of interest. All samples were equilibrated at the lowest temperature for 20 min before acquisition. An external bath circulator, connected to the infrared spectrometer, controlled the sample temperature. For temperature studies, samples were scanned using 2 °C intervals and a 2 min delay between each consecutive scan. The data were analyzed as previously described by Giudici et al. and Guillen et al. [34,35]. Subtraction of buffer spectra taken at the same temperature as the samples was performed interactively using either GRAMS/32 or SpectraCalc (Galactic Industries, Salem, MA) as described previously by Contreras et al. [36]. Frequencies at the center of gravity, when necessary, were measured by taking the top 10 points of each specific band and fitted to a Gaussian band. Band-narrowing strategies were applied to resolve the component bands in the Amide I′ region. Second-derivative spectra were calculated over a 15-data point range. Fourier self-deconvolution of the subtracted spectra was carried out using a Lorentzian shape and a triangular apodization with a resolution enhancement parameter, *K*, of 2.2, which is lower than log (signal/noise) and a full width at half-height of 18 cm^{-1} [37,38]. These parameters assumed that the spectra were not overdeconvolved as was evidenced by the absence of negative side lobes. Protein secondary structure elements were

quantified from curve-fitting analysis by band decomposition of the original Amide I′ band after spectral smoothing using the same software stated above [39]. Briefly, for each component, three parameters were considered: band position, band height, and bandwidth. The number and position of component bands were obtained through deconvolution and in decomposing the Amide I′ band, Gaussian components were used. The curve-fitting procedure was accomplished in two steps: in the first one, band position was fixed, allowing width and heights to approach final values, and in the second one, band positions were left to change. When necessary, these two steps were repeated. Band decomposition was performed using SpectraCalc (Galactic Industries, Salem, MA). The fitting result was evaluated visually by overlapping the reconstituted overall curve on the original spectrum and by examining the residual obtained by subtracting the fitting from the original curve. The procedure gave differences of less than 2% in band areas after the spectra were submitted to the curve fitting procedure. The frequency positions of the band centers were independently evaluated by second derivative procedures, being always very close to the positions found by deconvolution.

2.6. Steady-state fluorescence anisotropy

Aliquots of TMA-DPH or DPH in N,N′-dimethylformamide were directly added into MLVs formed in 10 mM Tris, 100 mM NaCl, 0.1 mM EDTA, and pH 7.4 to obtain a probe/lipid molar ratio of 1/500. Samples were incubated for 15 or 60 min when TMA-DPH or DPH was used, respectively, 10 °C above the gel to liquid crystalline phase transition temperature T_m of the phospholipid mixture. Afterwards, *St*Asp-PSI was added to obtain a lipid/protein molar ratio of 25:1 and incubated at 40 °C for 1 h, with occasional vortexing. All fluorescence studies were carried using 5 mm × 5 mm quartz cuvettes in a final volume of 400 μl (315 μM lipid concentration). The steady-state fluorescence anisotropy, <r>, was measured with an automated polarization accessory using a Varian Cary Eclipse fluorescence spectrometer, coupled to a Peltier for automatic temperature change. Samples were excited at 360 nm (slit width, 5 nm) and fluorescence emission was recorded at 430 nm (slit width, 5 nm). The data were analyzed as previously described by Moreno et al. [33].

2.7. Differential scanning calorimetry

MLVs were formed as stated above in 50 mM phosphate buffer, 25 mM NaCl, and pH 8. *St*Asp-PSI was added to obtain a lipid/protein molar ratio of 25:1. The final volume was 1.2 ml (0.5 mM lipid concentration) and incubated at 40 °C for 1 h with occasional vortexing. DSC experiments were performed in a VP-DSC differential scanning calorimeter (MicroCal LLC, MA) under a constant external pressure of 30 psi in order to avoid bubble formation, and samples were heated at a constant scan rate of 60 °C/h. Experimental data were corrected from small mismatches between the two cells by subtracting a buffer baseline prior to data analysis. The excess heat capacity functions were then analyzed by using Origin 7.0 (MicroCal Software). The thermograms were defined by the onset and completion temperatures of the transition peaks obtained from heating scans. In order to avoid artifacts due to the thermal history of the sample, the first scan was never considered; second and further scans were carried out until a reproducible and reversible pattern was obtained.

3. Results

3.1. Destabilization of negatively charged membranes

Previously, we showed the ability of *St*Asp-PSI to induce the release of trapped small fluorescent dyes (i.e., calcein and carboxyfluorescein) from negatively charged phospholipid bilayer vesicles composed of EPC/EPG (5:4) [29]. In order to determine the degree of destabilization of membranes induced by the interaction of *St*Asp-PSI, we analyzed the release of encapsulated FD70, a fluorescent probe with an average molecular weight of 70,000 and a Stokes radius of about 60 Å [40], in anionic model membranes. As shown in Fig. 1, *St*Asp-PSI was also able to induce leakage of fluorophores larger than carboxyfluorescein or calcein. Results obtained show that the initial rate and the maximal percentage of the FD70 release induced by *St*Asp-PSI were dose-dependent (Fig. 1), suggesting that *St*Asp-PSI can induce a great destabilization of the bilayer membrane, i.e., *St*Asp-PSI would induce the formation of pores having at least 60 Å diameter where FD70 molecules can leak out the vesicle. On the other hand, the leakage activity of *St*Asp-PSI was increased by extending the incubation time in the leakage assay, even at low concentrations (Fig. 1), suggesting a stronger dependence of the leakage effect on the time of interaction between the protein with the bilayers than on its concentration.

3.2. Secondary structure of StAsp-PSI

The existence of structural changes on *St*Asp-PSI induced by membrane binding was investigated by analyzing the infrared Amide I′ band located between 1700 and 1600 cm^{-1} by Fourier transform infrared spectroscopy (Fig. 2). The Amide I′ region of the fully hydrated *St*Asp-PSI in buffer is shown in Fig. 2A. The spectrum, at low temperature, was formed by a broad and relatively symmetric band with a maximum at about 1644 cm^{-1} which would mainly correspond to a mixture of unordered and helical structures [41]. Like with the circular dichroism results for *St*Asp-PSI reported by Bryksa et al. [42], the IR results for *St*Asp-PSI obtained here indicate a high degree of conformational stability of the protein in solution (Fig. 2A). However, another band at about 1620 cm^{-1} appeared in the spectrum at 40 °C, which increased in intensity as the temperature was raised. According to previous reports [41,43], this band should correspond to aggregated structures. These data suggest that *St*Asp-PSI changed from a mixture of helical and unordered structures at low temperatures to a mixture of helical, unordered and aggregated structures at high temperatures. Furthermore, this transitional change in overall structure occurs at about 45–50 °C (Fig. 2D).

In order to study any structural changes of *St*Asp-PSI when bounded to phospholipid membranes, samples containing both, phospholipids and *St*Asp-PSI, were prepared as described in Materials and methods. Results obtained show that in the presence of either DMPC or DMPG, the Amide I′ envelope of *St*Asp-PSI was rather similar to that found for the protein in solution at all temperatures assayed (Fig. 2B and C, respectively). These data would suggest that not significant changes in the structure of *St*Asp-PSI were induced by its interaction with the membrane.

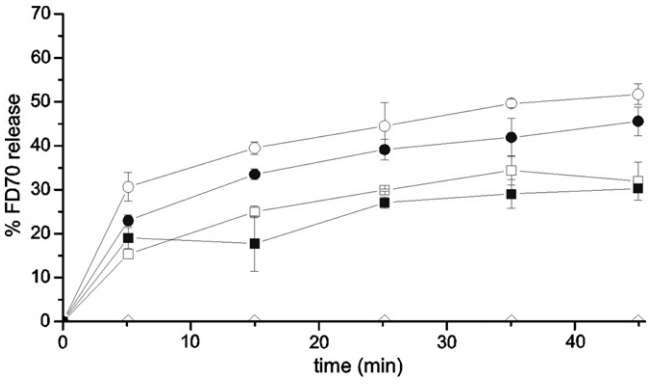

Fig. 1. Effect of *St*Asp-PSI on the release of FD70 fluorescent dye from membranes composed of EPC/EPG at a molar ratio of 5:4 and pH 7. The *St*Asp-PSI concentrations used were 0 μM (◊), 1.25 μM (■), 2.48 μM (□), 5 μM (●), and 8.26 μM (○). Error bars indicate standard deviations of the mean of triplicate samples.

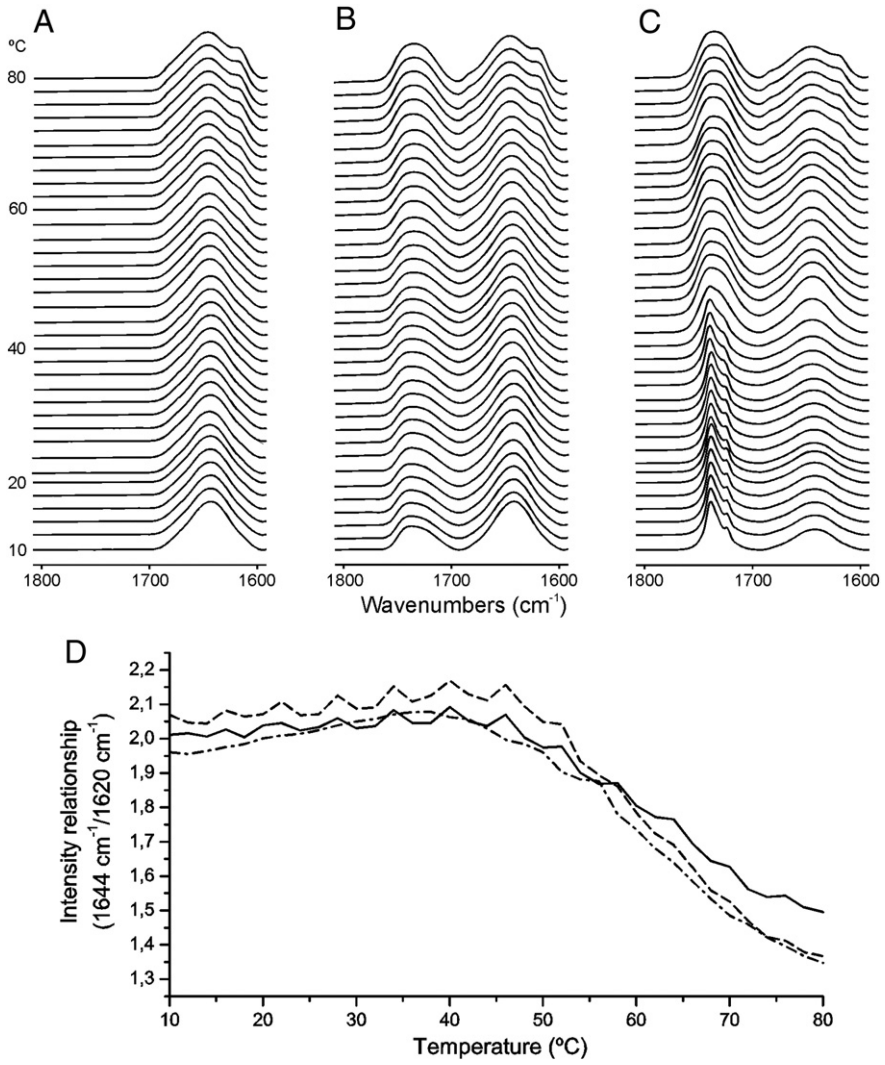

Fig. 2. Stacked infrared spectra in the C═O and Amide I′ region for *St*Asp-PSI in solution (A) and in the presence of DMPC (B) and DMPG (C) at different temperatures as indicated. The phospholipid/protein molar ratio was 50:1. The temperature dependence of the 1644 cm^{-1}/1620 cm^{-1} intensity relationship for *St*Asp-PSI in solution (-) and in the presence of DMPC (- - -) and DMPG (-·-) are shown in panel D. See text for details.

To observe the underlying components of the broad Amide I′ band of *St*Asp-PSI, we have applied several enhancement methods, such as self-deconvolution and derivative methods, to the original envelope as well as decomposition of the Amide I′ infrared band [37]. Analysis of *St*Asp-PSI in solution shows component bands with frequencies of 1672, 1657, 1645, 1631 and 1615 cm^{-1} (Fig. 3A). We have analyzed the results obtained taking into account that the band appearing at 1672 cm^{-1} is due to turns, the band at 1657 cm^{-1} to α-helix, the band at 1645 cm^{-1} to either random or α-helix or both, the band at 1631 cm^{-1} to β-sheet, and the band at 1615 cm^{-1} would correspond to amino acid side chain vibrations [44–48]. The secondary structure of the protein in solution and at 20 °C would consist of about 13% of turns, 26% of α-helix, 28% of either random or α-helix or both and 33% of β-sheet (Table 1). Therefore, the results acquired here are in agreement with previous results obtained from the circular dichroism analysis of *St*Asp-PSI. These analyses showed that *St*Asp-PSI adopts a similar secondary structure reported for other SAPLIPs that include a high content of α-helix (approximately 54%) [21,29,49,50]. The same number of bands with similar frequencies was identified for *St*Asp-PSI in the presence of zwitterionic and anionic membranes. However, the interaction of *St*Asp-PSI with membranes composed of either DMPC or DMPG (Fig. 3B and C, respectively) leads to an increase of the band intensity corresponding to either random or α-helix or both structures from 28% to 35% for DMPC membranes and to 36% for DMPG membranes (Table 1). As shown above, no dramatic changes in the structure of *St*Asp-PSI on binding to the phospholipid membranes were detected.

3.3. Effects of StAsp-PSI on the structural and thermotropic properties of membranes

Membrane lipids undergo a cooperative melting reaction, which is linked to the loss of conformational order of the lipid chains and it has been known for a long time that the melting process of membrane lipids is influenced by many types of molecules including proteins and peptides. The effect of *St*Asp-PSI on the structural and thermotropic properties of phospholipid membranes was investigated by measuring the steady-state fluorescence anisotropy of the fluorescent probes DPH and TMA-DPH incorporated into model membranes composed of saturated synthetic phospholipids as a function of temperature (Fig. 4). DPH is known to partition mainly into the hydrophobic core of the membrane, whereas TMA-DPH is oriented at the membrane bilayer with its charge localized at the lipid–water interface [36]. Their different locations and orientations in the membrane allow analyzing the effect of *St*Asp-PSI on the structural and thermotropic properties along the full length of the membrane. For DMPG and DMPS, *St*Asp-PSI decreased significantly the cooperativity of the thermal transition and in addition

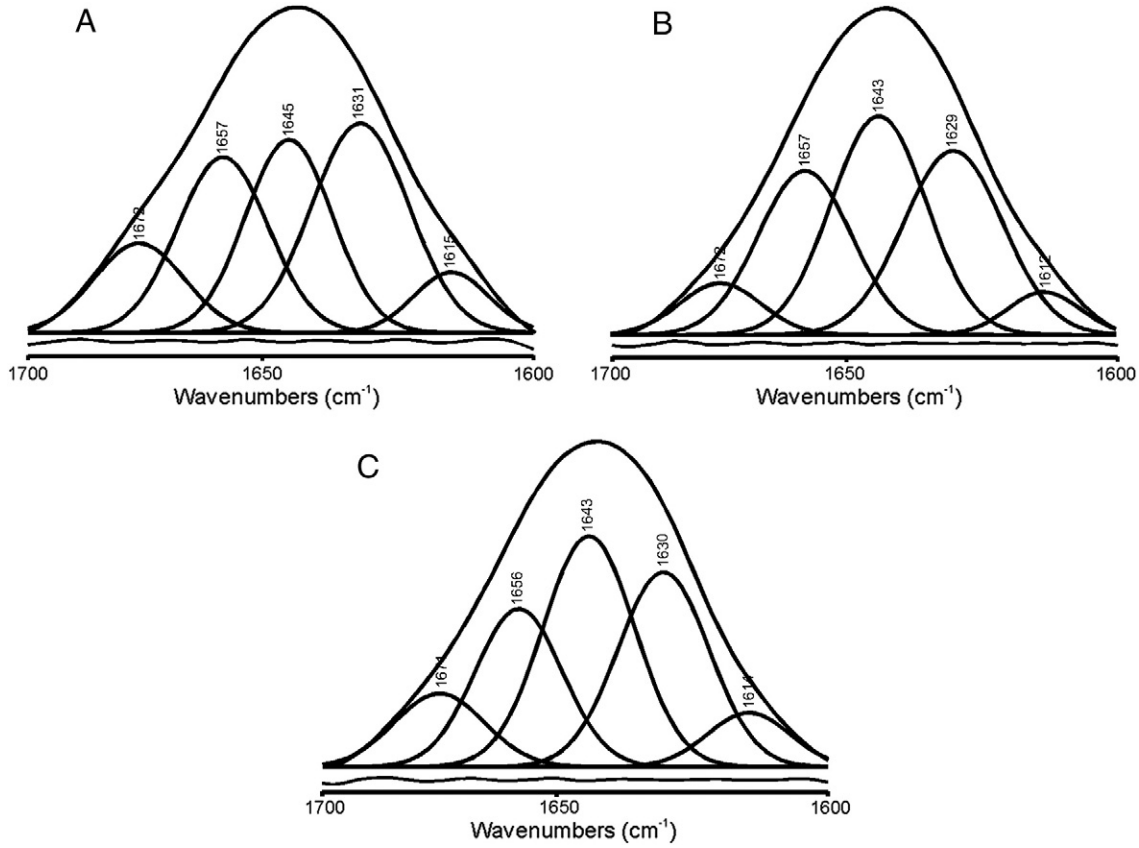

Fig. 3. Amide I′ band decomposition of *St*Asp-PSI in solution (A) and in the presence of DMPC (B) and DMPG (C) at an original phospholipid/protein molar ratio of 50:1 in D_2O buffer at 20 °C. The component bands, the envelope, and the difference between the fitted curve and the original spectrum are shown.

elicited a shift of about 2–5 °C to higher temperatures of the T_m (Fig. 4A, B, C and D). On the other hand, *St*Asp-PSI produced a significant change in the anisotropy both below and above the main transition temperature on DMPG and DMPS in the presence of both fluorescent probes. When DMPC membranes were used, *St*Asp-PSI did not produce any changes in the cooperativity of the phospholipid, although a slight shift of T_m to higher temperatures was detected. This effect was higher for TMA-DPH than for DPH (Fig. 4E and F). These results suggest that, *St*Asp-PSI is able to perturb the phospholipid acyl chains of negatively charged phospholipids. According to already reported data [51], our results suggest that protein incorporation into the lipid bilayer is affected by the difference in charge between the phospholipid head groups. Therefore, *St*Asp-PSI should be primarily located at the lipid–water interface influencing the fluidity of the phospholipids.

3.4. Effects of StAsp-PSI on the thermotropic phase behavior of MLVs

Differential scanning calorimetry (DSC) is a powerful, non-perturbing thermodynamic technique which has proven very useful for studies of lipid–protein interactions in model and biological membranes in general and for the study of the interactions of AMPs with lipid bilayer model membranes in particular [52–54]. We have used DSC to analyze the effect of *St*Asp-PSI on the thermotropic phase behavior of the major phospholipid classes of bacterial and animal cells. Since PCs are virtually absent in bacterial membranes but are generally the most abundant phospholipid class in eukaryotic plasma membrane, DMPC bilayers can serve as a model for the surface membrane of the cells of higher animals, especially as PCs are typically localized primarily in the outer monolayer of the lipid bilayer of such membranes. On the other hand, PGs are absent from eukaryotic plasma membranes, but are ubiquitous and often abundant in prokaryotic surface membranes and responsible for their negative charge [55]. The effect of *St*Asp-PSI on the thermotropic phase behavior of multilamellar vesicles (MLVs) with different compositions (DMPC, DMPG, and DMPS) is shown in Fig. 5. Results obtained demonstrate that, in the absence of *St*Asp-PSI, DMPC and DMPG exhibit two endothermic events on heating. A weak energetic pretransition, corresponding to the melting of the lipid headgroups, was observed at 14 °C for DMPC and 11 °C for DMPG, and a strong energetic main phase transition near 24 and 23 °C respectively, corresponding to the highly cooperative gel/liquid-crystalline

Table 1
Secondary structure content, in %, of *St*Asp-PSI in different environments as determined by FTIR.[a]

Structural assignment[b]	% Turns (band at ~1672 cm^{-1})	% α-Helix (band at ~1657 cm^{-1})	% Random/α-helix (band at ~1645 cm^{-1})	β-Sheet (band at ~1631 cm^{-1})
*St*Asp-PSI (in solution)	13[c]	26	28	33
*St*Asp-PSI + DMPC	8	26	35	31
*St*Asp-PSI + DMPG	11	23	36	30

[a] Errors in the band areas are estimated to be ±2 cm^{-1} (see text for details).
[b] There is a band centered at about 1615 cm^{-1}, assigned to amino acid side chains, which has not been taken into account to determine the percentage of secondary structure.
[c] Values are rounded off to the nearest integer.

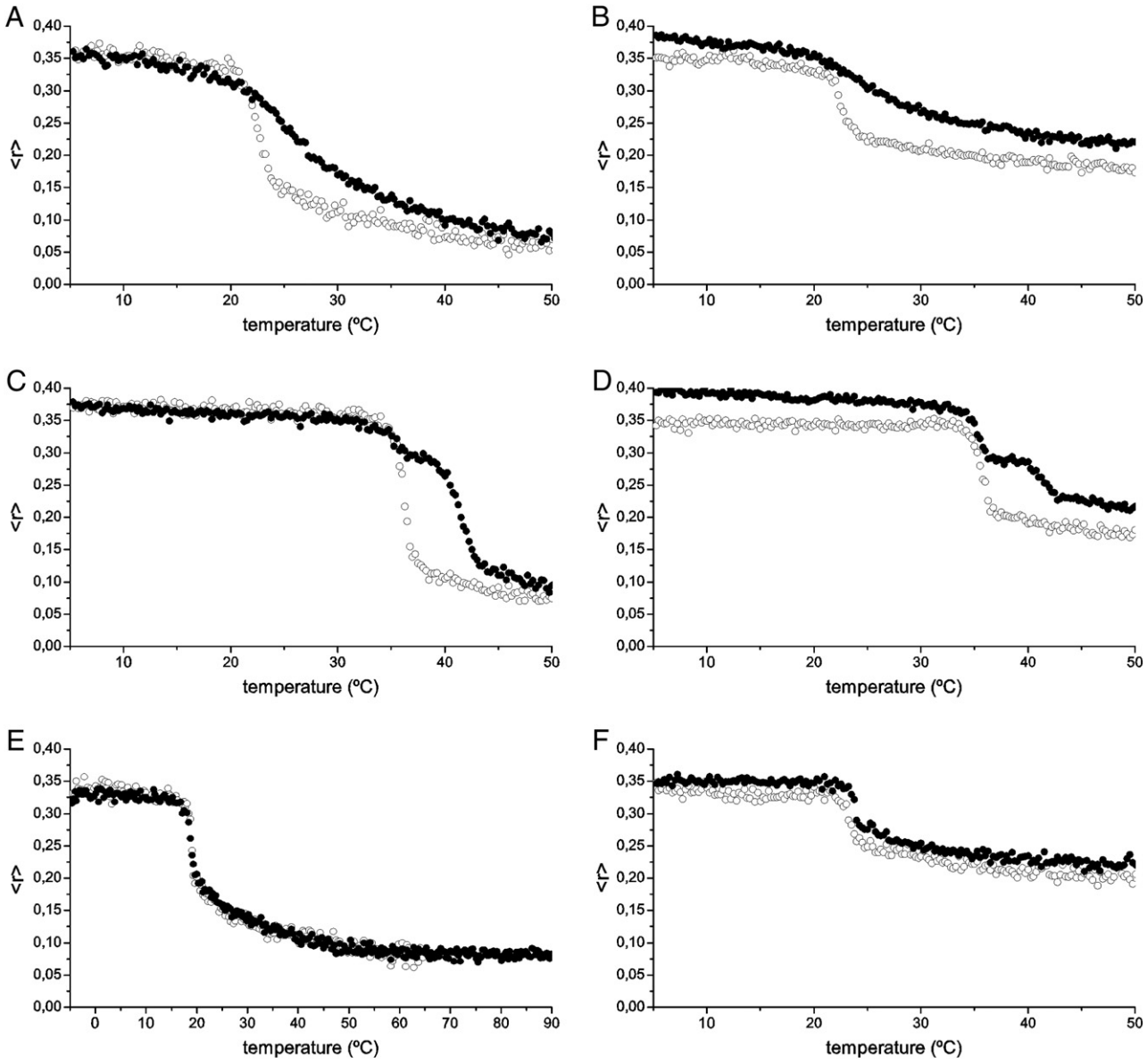

Fig. 4. Steady-state anisotropy, <r>, of DPH (A, C and E) and TMA-DPH (B, D and F) incorporated into DMPG (A and B), DMPS (C and D) and DMPC (E and F) model membranes as a function of temperature. Data correspond to vesicles containing pure phospholipids (○) and phospholipids plus *St*Asp-PSI at a 25:1 molar ratio (●).

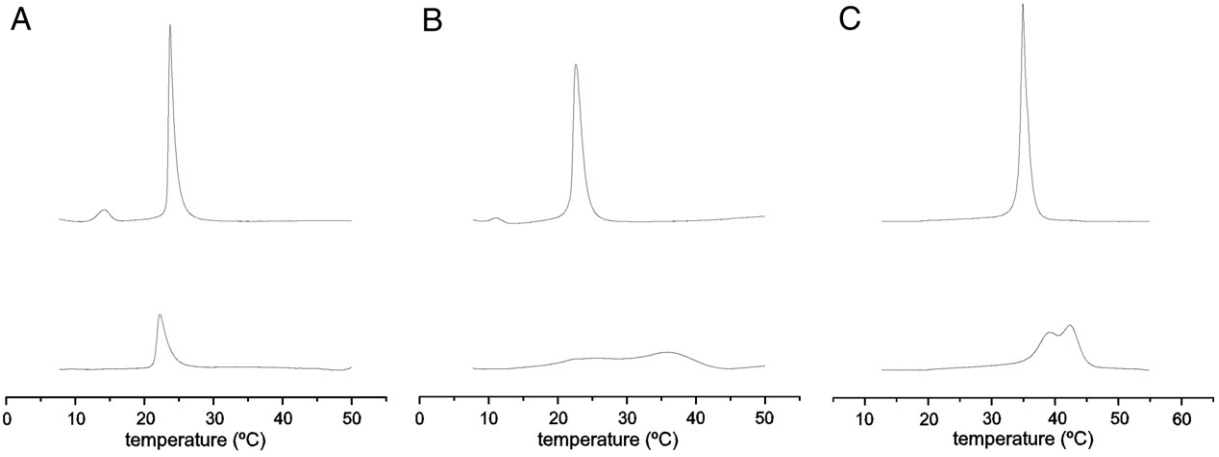

Fig. 5. Differential scanning calorimetry heating-scan thermograms for model membranes composed of DMPC (A), DMPG (B) and DMPS (C) in the absence (upper curves) and in the presence (lower curves) of *St*Asp-PSI at a phospholipid/protein molar ratio of 25:1. All thermograms were normalized to the same amount of phospholipid.

(chain melting) transition of the lipid side chains (Fig. 5A and B). On the other hand, DMPS exhibits a single endothermic transition at approximately 35 °C, which corresponds to the highly cooperative gel/liquid-crystalline phase transition of the lipid (Fig. 5C). In the presence of *St*Asp-PSI, the thermotropic phase behavior of DMPC was significantly modified, since the pretransition disappeared and the enthalpy of the main phase transition was reduced. For both anionic phospholipids DMPG and DMPS, the presence of *St*Asp-PSI significantly broadened the transition of the phospholipids in accordance with the anisotropy results described above (Fig. 5B and C). Moreover, the main transition is apparently composed of at least two different peaks, which should be due to mixed phases (T_m of 22.2 and 35.9 °C for DMPG and 38.9 and 42.3 °C for DMPS). The coexistence of at least two phases would indicate that one of them would be enriched in *St*Asp-PSI (phospholipids highly disturbed) whereas the other one would be impoverished in it (phospholipids slightly disturbed).

4. Discussion

Induced permeabilization of cell membranes is one of the most common killing mechanisms produced by antimicrobial proteins and peptides (AMPs) [56,57]. In this work we have analyzed the structural and dynamic features which might be relevant for membrane disruption during *St*Asp-PSI–membrane interaction.

For several peptides, formation of multimeric pores has been suggested to be responsible for membrane permeabilization [58–62]. A peptide that forms pores, defined as passageways of any kind that have limited apertures, will lead to leakage of vesicle contents in a manner that depends on the size of the solute [57]. If, however, the peptide acts in a detergent-like manner and micellizes the membrane, there should be no preference in the release of markers of different sizes [57]. In this work, results obtained from leakage assays suggest that the release of size-marker molecules from vesicles composed of EPC/EPG is related to the *St*Asp-PSI concentration. Since, for large size molecules such as FD70, a 50% of leakage was observed at a *St*Asp-PSI amount 3-folds higher (8.5 μM) than the necessary *St*Asp-PSI amount to produce the same effect when smaller fluorophores (i.e., calcein and carboxyfluorescein) were used (2.5 μM) [29]. Like the results previously reported by Benachir and Lafleur [63], these results could indicate that the *St*Asp-PSI mechanism involved in vesicle membrane disruption includes pore formation.

Prepore formation is a prerequisite for membrane insertion; however, monomers can effectively enter into the membrane [62]. By this way, protein monomers insert into the bilayer and subsequently diffuse laterally in the membrane to assemble into multimers to form pores [64–66]. Here we show that the leakage activity of *St*Asp-PSI is significantly increased by extending the time of incubation in the leakage assays, even at the lowest concentration assayed. This data suggests that vesicle membrane disruption produced by *St*Asp-PSI is also dependent of the time of interaction between this protein and the phospholipid bilayers. To other AMPs this temporal delay has been related with lateral diffusion of the monomers to assemble into aggregates [67]. However, other assays are necessary to corroborate this relationship.

The infrared spectra of the Amide I′ region of the fully hydrated *St*Asp-PSI in solution at low temperatures displayed a coexistence of α-helix and random structures; however, a broad transition with a concomitant increase in aggregated structures occurred at about 45 °C. On the other hand, we have attempted to analyze the possible structural changes in *St*Asp-PSI induced by the interaction with membranes of different types of phospholipids. Analysis of IR data indicates that, in the presence of lipid vesicles containing DMPG or DMPC, *St*Asp-PSI undergoes slight changes in its secondary structure. These changes mainly consist in an increase in the content of either random or α-helix or both structures. That kind of structural changes has been shown to involve a highly dynamic association–dissociation mechanism for several peptides inducing conformational changes in the peptides bound to membranes and possible self-association [29,68]. The loss of leakage, fusogenic and cytotoxic activities of *St*Asp-PSI in the presence of DTT has been previously reported [20,23,29,42]. Additionally, we have determined the importance of intermolecular disulfide bonds to produce *St*Asp-PSI monomer association in the presence of the phospholipid vesicles [29]. All these results could suggest that the presence of

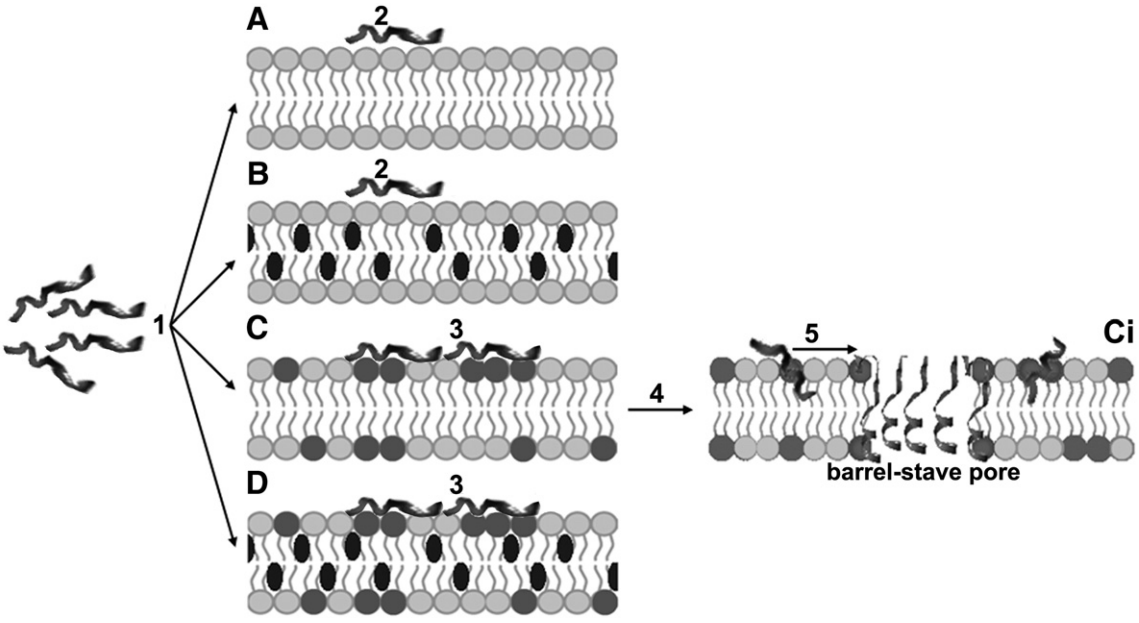

Fig. 6. Schematic overview of the possible mechanism of interaction of *St*Asp-PSI with membranes. *St*Asp-PSI in monomer form comes close to the membrane target (1). In zwitterionic membranes (A, B), positively charged residues of *St*Asp-PSI interact weakly with the head group of phospholipids (2). In anionic membranes (C, D), they interact strongly with the head group of the negative phospholipids (3); insertion of the proteins into the membrane interface (4); lateral diffusion in the membrane (5); and finally conformational changes of *St*Asp-PSI leading to aggregation necessary for peptide induced pore formation. In membranes composed of PG or PS (Ci), *St*Asp-PSI could insert deeply into the bilayer to form a barrel-stave pore structure. The presence of cholesterol in zwitterionic (B) and anionic (D) membranes prevents lateral diffusion of *St*Asp-PSI in the membrane. *St*Asp-PSI is represented by ribbons. The head groups of zwitterionic phospholipids are colored in light gray and the head groups of negatively charged phospholipids are colored in dark gray. Cholesterol is represented by black ellipses.

intermolecular disulfide bonds is critical to *St*Asp-PSI self-association into the membrane to produce its disruption by pore formation.

Also, we have shown that *St*Asp-PSI is able to affect the steady-state fluorescence anisotropy of fluorescent probes located into the palisade structure of the membrane, since the protein was able to decrease the mobility and transition cooperativity of the phospholipid acyl chains of anionic membranes composed of DMPG and DMPS when compared to the pure phospholipids. No changes were observed in the structure of zwitterionic membranes in the presence of *St*Asp-PSI. Interestingly, these data suggest that the insertion of *St*Asp-PSI into the bilayer palisade depends on phospholipid composition.

Calorimetry experiments further corroborated these results, and additionally indicated that *St*Asp-PSI induced the presence of mixed lipid phases, enriched or impoverished in protein. This result strengthens that the location of *St*Asp-PSI is at or near the membrane interface, influencing the fluidity of the phospholipids. It has also been described, for other proteins and peptides, that an increase in gel phase disorder and a decrease in the gel to liquid phase transition cooperativity are related to the insertion of the protein into the membrane and thus the spreading of the phosphate groups [69–72]. Additionally, *St*Asp-PSI could insert deeply into the bilayer to form a barrel-stave pore structure in membranes composed of DMPG and DMPS, since *St*Asp-PSI was able to perturb the phospholipid acyl chains in membranes with these compositions.

Nowadays, the interest on the study of antimicrobial peptides and proteins has increased because of the microbial resistance developed toward many antimicrobial compounds [73–75]. Many of these antimicrobial peptides not only perturb and disrupt microbial cell membranes, but they are also lytic to eukaryotic ones. The understanding of their mechanism of action is therefore essential to provide a basis for the design of peptides with a directed action toward specific cell types. The results obtained here can be related to the selective cytotoxic activity of *St*APs and *St*Asp-PSI, since they interact differently with distinct types of cells because of differences in phospholipid membrane composition [20,23,24,29].

Definitive demonstration of the mode of peptide disruption of a bilayer is difficult for an experiment model, especially as a single peptide may exhibit more than one mode of interaction with the bilayer [76]. Nevertheless, the results we have discussed here complement other studies that we have done previously on *St*Asp-PSI [20,29]. Taking this into account, in Fig. 6 we propose a model of interaction of *St*Asp-PSI with phospholipid membranes of different compositions. In this model we suggest that *St*Asp-PSI interacts in a complex, conformationally dependent, way with phospholipid membranes, involving a number of processes, being the first one an electrostatic interaction with negatively charged phospholipids, then insertion of the proteins into the membrane interface, lateral diffusion in the membrane and finally aggregation, leading to the disruption of the membrane by a pore formation.

Acknowledgements

This work was supported in part by grant BFU2008-02617-BMC (Ministerio de Ciencia y Tecnología, Spain) to J.V.; National Scientific and Technical Research Council (CONICET) grant to M.G.G.; Scientific Research Commission of the Province of Buenos Aires (CIC) grant to G.D. and University of Mar del Plata grant to G.D. and M.G.G. F.M. is fellow of CONICET; G.D. is an established researcher of CIC and M.G.G. is an established researcher of CONICET. F.M. is grateful for a fellowship (MAEC-AECI 2009–2010) of the Spanish Ministry of Foreign Affairs and Cooperation.

References

[1] W.C. Wimley, K. Hristova, Antimicrobial peptides: successes, challenges and unanswered questions, J. Membr. Biol. 239 (2011) 27–34.
[2] Y. Li, Q. Xiang, Q. Zhang, Y. Huang, Z. Su, Overview on the recent study of antimicrobial peptides: origins, functions, relative mechanisms and application, Peptides 37 (2012) 207–215.
[3] K.A. Brogden, Antimicrobial peptides: pore formers or metabolic inhibitors in bacteria? Nat. Rev. Microbiol. 3 (2005) 238–250.
[4] H.G. Boman, Innate immunity and the normal microflora, Immunol. Rev. 173 (2000) 5–16.
[5] M. Zasloff, Reconstructing one of nature's designs, Trends Pharmacol. Sci. 21 (2000) 236–238.
[6] F. Garcia-Olmedo, A. Molina, J.M. Alamillo, P. Rodriguez-Palenzuela, Plant defense peptides, Biopolymers 47 (1998) 479–491.
[7] J.X. Yan, K.R. Wang, R. Chen, J.J. Song, B.Z. Zhang, W. Dang, W. Zhang, R. Wang, Membrane active antitumor activity of NK-18, a mammalian NK-lysin-derived cationic antimicrobial peptide, Biochimie 94 (2012) 184–191.
[8] K.L. Brown, R.E. Hancock, Cationic host defense (antimicrobial) peptides, Curr. Opin. Immunol. 18 (2006) 24–30.
[9] S.J. Kang, D.H. Kim, T. Mishig-Ochir, B.J. Lee, Antimicrobial peptides: their physicochemical properties and therapeutic application, Arch. Pharm. Res. 35 (2012) 409–413.
[10] A. Giuliani, G. Pirri, A. Bozzi, A. Di Giulio, M. Aschi, A.C. Rinaldi, Antimicrobial peptides: natural templates for synthetic membrane-active compounds, Cell. Mol. Life Sci. 65 (2008) 2450–2460.
[11] H. Uvell, Y. Engstrom, A multilayered defense against infection: combinatorial control of insect immune genes, Trends Genet. 23 (2007) 342–349.
[12] D.R. Davies, The structure and function of the aspartic proteinases, Annu. Rev. Biophys. Biophys. Chem. 19 (1990) 189–215.
[13] N.D. Rawlings, A.J. Barrett, Families of aspartic peptidases, and those of unknown catalytic mechanism, Methods Enzymol. 248 (1995) 105–120.
[14] A. Mutlu, S. Gal, Plant aspartic proteinases: enzymes on the way to a function, Physiol. Plant. 105 (1999) 569–576.
[15] I. Simoes, C. Faro, Structure and function of plant aspartic proteinases, Eur. J. Biochem. 271 (2004) 2067–2075.
[16] F. Chen, M. Fooland, Molecular organization of a gene in barley which encodes a protein similar to aspartic protease and its specific expression in nucellar cells during degeneration, Plant Mol. Biol. 35 (1997) 821–831.
[17] Y. Xia, H. Suzuki, J. Borevitz, J. Blount, Z. Guo, K. Patel, R.A. Dixon, C. Lamb, An extracellular aspartic protease functions in *Arabidopsis* disease resistance signaling, EMBO J. 23 (2004) 980–988.
[18] K. Guruprasad, K. Tormakangas, J. Kervinen, T.L. Blundell, Comparative modelling of barley-grain aspartic proteinase: a structural rationale for observed hydrolytic specificity, FEBS Lett. 352 (1994) 131–136.
[19] A.M. Vaccaro, M. Tatti, F. Ciaffoni, R. Salvioli, B. Maras, A. Barca, Function of saposin C in the reconstitution of glucosylceramidase by phosphatidylserine liposomes, FEBS Lett. 336 (1993) 159–162.
[20] F.F. Muñoz, J.R. Mendieta, M.R. Pagano, R.A. Paggi, G.R. Daleo, M.G. Guevara, The swaposin-like domain of potato aspartic protease (StAsp-PSI) exerts antimicrobial activity on plant and human pathogens, Peptides 31 (2010) 777–785.
[21] H. Bruhn, A short guided tour through functional and structural features of saposin-like proteins, Biochem. J. 389 (2005) 249–257.
[22] G. Wang, X. Li, Z. Wang, APD2: the updated antimicrobial peptide database and its application in peptide design, Nucleic Acids Res. 37 (2009) D933–D937.
[23] J.R. Mendieta, M.R. Pagano, F.F. Munoz, G.R. Daleo, M.G. Guevara, Antimicrobial activity of potato aspartic proteases (StAPs) involves membrane permeabilization, Microbiology 152 (2006) 2039–2047.
[24] J.R. Mendieta, C. Fimognari, G.R. Daleo, P. Hrelia, M.G. Guevara, Cytotoxic effect of potato aspartic proteases (StAPs) on Jurkat T cells, Fitoterapia 81 (2010) 329–335.
[25] M. Guevara, C. Oliva, M. Machinandiarena, G. Daleo, Purification and properties of an aspartic protease from potato tuber that is inhibited by a basic chitinase, Physiol. Plant. 106 (1999) 164–169.
[26] M.G. Guevara, C. Almeida, J.R. Mendieta, C.J. Faro, P. Verissimo, E.V. Pires, G.R. Daleo, Molecular cloning of a potato leaf cDNA encoding an aspartic protease (StAsp) and its expression after *P. infestans* infection, Plant Physiol. Biochem. 43 (2005) 882–889.
[27] M. Guevara, C. Oliva, M. Huarte, G. Daleo, An aspartic protease with antimicrobial activity is induced after infection and wounding in intercellular fluids of potato tubers, Eur. J. Plant Pathol. 108 (2002) 131–137.
[28] M. Guevara, P. Veríssimo, E. Pires, G. Daleo, Potato aspartic proteases: induction, antimicrobial activity and substrate specificity, J. Plant Pathol. 86 (2004) 233–238.
[29] F. Muñoz, M.F. Palomares-Jerez, G. Daleo, J. Villalain, M.G. Guevara, Cholesterol and membrane phospholipid compositions modulate the leakage capacity of the swaposin domain from a potato aspartic protease (StAsp-PSI), Biochim. Biophys. Acta 1811 (2011) 1038–1044.
[30] P.K. Smith, R.I. Krohn, G.T. Hermanson, A.K. Mallia, F.H. Gartner, M.D. Provenzano, E.K. Fujimoto, N.M. Goeke, B.J. Olson, D.C. Klenk, Measurement of protein using bicinchoninic acid, Anal. Biochem. 150 (1985) 76–85.
[31] L.D. Mayer, M.J. Hope, P.R. Cullis, Vesicles of variable sizes produced by a rapid extrusion procedure, Biochim. Biophys. Acta 858 (1986) 161–168.
[32] A. Bernabeu, J. Guillen, A.J. Perez-Berna, M.R. Moreno, J. Villalain, Structure of the C-terminal domain of the pro-apoptotic protein Hrk and its interaction with model membranes, Biochim. Biophys. Acta 1768 (2007) 1659–1670.
[33] M.R. Moreno, J. Guillen, A.J. Perez-Berna, D. Amoros, A.I. Gomez, A. Bernabeu, J. Villalain, Characterization of the interaction of two peptides from the N terminus of the NHR domain of HIV-1 gp41 with phospholipid membranes, Biochemistry 46 (2007) 10572–10584.
[34] M. Giudici, R. Pascual, L. de la Canal, K. Pfuller, U. Pfuller, J. Villalain, Interaction of viscotoxins A3 and B with membrane model systems: implications to their mechanism of action, Biophys. J. 85 (2003) 971–981.

[35] J. Guillen, M.R. Moreno, A.J. Perez-Berna, A. Bernabeu, J. Villalain, Interaction of a peptide from the pre-transmembrane domain of the severe acute respiratory syndrome coronavirus spike protein with phospholipid membranes, J. Phys. Chem. B 111 (2007) 13714–13725.
[36] L.M. Contreras, F.J. Aranda, F. Gavilanes, J.M. Gonzalez-Ros, J. Villalain, Structure and interaction with membrane model systems of a peptide derived from the major epitope region of HIV protein gp41: implications on viral fusion mechanism, Biochemistry 40 (2001) 3196–3207.
[37] J.K. Kauppinen, D.J. Moffatt, D.G. Cameron, H.H. Mantsch, Noise in Fourier self-deconvolution, Appl. Opt. 20 (1981) 1866–1879.
[38] H.H. Mantsch, P.W. Yang, A. Martin, D.G. Cameron, Infrared spectroscopic studies of *Acholeplasma laidlawaii* B membranes. Comparison of the gel to liquid-crystal phase transition in intact cells and isolated membranes, Eur. J. Biochem. 178 (1988) 335–341.
[39] S. Bañuelos, J.L. Arrondo, F.M. Goñi, G. Pifat, Surface–core relationships in human low density lipoprotein as studied by infrared spectroscopy, J. Biol. Chem. 270 (1995) 9192–9196.
[40] T.C. Laurent, K.A. Granath, Fractionation of dextran and Ficoll by chromatography on Sephadex G-200, Biochim. Biophys. Acta 136 (1967) 191–198.
[41] D.M. Byler, H. Susi, Examination of the secondary structure of proteins by deconvolved FTIR spectra, Biopolymers 25 (1986) 469–487.
[42] B.C. Bryksa, P. Bhaumik, E. Magracheva, D.C. De Moura, M. Kurylowicz, A. Zdanov, J.R. Dutcher, A. Wlodawer, R.Y. Yada, Structure and mechanism of the saposin-like domain of a plant aspartic protease, J. Biol. Chem. 286 (2011) 28265–28275.
[43] J.L. Arrondo, F.M. Goñi, Structure and dynamics of membrane proteins as studied by infrared spectroscopy, Prog. Biophys. Mol. Biol. 72 (1999) 367–405.
[44] J.L. Arrondo, H.H. Mantsch, N. Mullner, S. Pikula, A. Martonosi, Infrared spectroscopic characterization of the structural changes connected with the E1–E2 transition in the Ca2+-ATPase of sarcoplasmic reticulum, J. Biol. Chem. 262 (1987) 9037–9043.
[45] J.L. Arrondo, A. Muga, J. Castresana, F.M. Goni, Quantitative studies of the structure of proteins in solution by Fourier-transform infrared spectroscopy, Prog. Biophys. Mol. Biol. 59 (1993) 23–56.
[46] G.A. Ascoli, K.X. Luu, J.L. Olds, T.J. Nelson, P.A. Gusev, C. Bertucci, E. Bramanti, A. Raffaelli, P. Salvadori, D.L. Alkon, Secondary structure and Ca2+-induced conformational change of calexcitin, a learning-associated protein, J. Biol. Chem. 272 (1997) 24771–24779.
[47] R. Vila, I. Ponte, M. Collado, J.L. Arrondo, P. Suau, Induction of secondary structure in a COOH-terminal peptide of histone H1 by interaction with the DNA: an infrared spectroscopy study, J. Biol. Chem. 276 (2001) 30898–30903.
[48] W.K. Surewicz, H.H. Mantsch, D. Chapman, Determination of protein secondary structure by Fourier transform infrared spectroscopy: a critical assessment, Biochemistry 32 (1993) 389–394.
[49] D. Anderson, M. Sawaya, D. Cascio, W. Ernst, R. Modlin, A. Krensky, D. Eisenberg, Granulysin cristal structure and a structure-derived lytic mechanism, J. Mol. Biol. 325 (2003) 355–365.
[50] E. de Alba, S. Weiler, N. Tjandra, Solution structure of human saposin C: pH-dependent interaction with phospholipid vesicles, Biochemistry 42 (2003) 14729–14740.
[51] M.F. Palomares-Jerez, J. Villalain, Membrane interaction of segment H1 (NS4B(H1)) from hepatitis C virus non-structural protein 4B, Biochim. Biophys. Acta 1808 (2011) 1219–1229.
[52] E.J. Prenner, R.N. Lewis, L.H. Kondejewski, R.S. Hodges, R.N. McElhaney, Differential scanning calorimetric study of the effect of the antimicrobial peptide gramicidin S on the thermotropic phase behavior of phosphatidylcholine, phosphatidylethanolamine and phosphatidylglycerol lipid bilayer membranes, Biochim. Biophys. Acta 1417 (1999) 211–223.
[53] R.N. McElhaney, Differential scanning calorimetric studies of lipid–protein interactions in model membrane systems, Biochim. Biophys. Acta 864 (1986) 361–421.
[54] K. Lohner, E.J. Prenner, Differential scanning calorimetry and X-ray diffraction studies of the specificity of the interaction of antimicrobial peptides with membrane-mimetic systems, Biochim. Biophys. Acta 1462 (1999) 141–156.
[55] G.W. Seto, S. Marwaha, D.M. Kobewka, R.N. Lewis, F. Separovic, R.N. McElhaney, Interactions of the Australian tree frog antimicrobial peptides aurein 1.2, citropin 1.1 and maculatin 1.1 with lipid model membranes: differential scanning calorimetric and Fourier transform infrared spectroscopic studies, Biochim. Biophys. Acta 1768 (2007) 2787–2800.
[56] V. Teixeira, M.J. Feio, M. Bastos, Role of lipids in the interaction of antimicrobial peptides with membranes, Prog. Lipid Res. 51 (2012) 149–177.
[57] A.S. Ladokhin, M.E. Selsted, S.H. White, Sizing membrane pores in lipid vesicles by leakage of co-encapsulated markers: pore formation by melittin, Biophys. J. 72 (1997) 1762–1766.
[58] D. Rapaport, R. Peled, S. Nir, Y. Shai, Reversible surface aggregation in pore formation by pardaxin, Biophys. J. 70 (1996) 2502–2512.
[59] S. Rex, Pore formation induced by the peptide melittin in different lipid vesicle membranes, Biophys. Chem. 58 (1996) 75–85.
[60] G. Schwarz, A. Arbuzova, Pore kinetics reflected in the dequenching of a lipid vesicle entrapped fluorescent dye, Biochim. Biophys. Acta 1239 (1995) 51–57.
[61] W.C. Wimley, M.E. Selsted, S.H. White, Interactions between human defensins and lipid bilayers: evidence for formation of multimeric pores, Protein Sci. 3 (1994) 1362–1373.
[62] N. Groulx, H. McGuire, R. Laprade, J.L. Schwartz, R. Blunck, Single molecule fluorescence study of the Bacillus thuringiensis toxin Cry1Aa reveals tetramerization, J. Biol. Chem. 286 (2011) 42274–42282.
[63] T. Benachir, M. Lafleur, Study of vesicle leakage induced by melittin, Biochim. Biophys. Acta 1235 (1995) 452–460.
[64] M.Z. Haider, D.J. Ellar, Mechanism of action of *Bacillus thuringiensis* insecticidal delta-endotoxin: interaction with phospholipid vesicles, Biochim. Biophys. Acta 978 (1989) 216–222.
[65] A.I. Aronson, Y. Shai, Why *Bacillus thuringiensis* insecticidal toxins are so effective: unique features of their mode of action, FEMS Microbiol. Lett. 195 (2001) 1–8.
[66] N.J. Tigue, J. Jacoby, D.J. Ellar, The alpha-helix 4 residue, Asn135, is involved in the oligomerization of Cry1Ac1 and Cry1Ab5 *Bacillus thuringiensis* toxins, Appl. Environ. Microbiol. 67 (2001) 5715–5720.
[67] P. Koszalka, E. Kamysz, M. Wejda, W. Kamysz, J. Bigda, Antitumor activity of antimicrobial peptides against U937 histiocytic cell line, Acta Biochim. Pol. 58 (2011) 111–117.
[68] P.F. Almeida, A. Pokorny, Mechanisms of antimicrobial, cytolytic, and cell-penetrating peptides: from kinetics to thermodynamics, Biochemistry 48 (2009) 8083–8093.
[69] F. Yoneyama, Y. Imura, K. Ohno, T. Zendo, J. Nakayama, K. Matsuzaki, K. Sonomoto, Peptide–lipid huge toroidal pore, a new antimicrobial mechanism mediated by a lactococcal bacteriocin, lacticin Q, Antimicrob. Agents Chemother. 53 (2009) 3211–3217.
[70] D. Sengupta, H. Leontiadou, A.E. Mark, S.J. Marrink, Toroidal pores formed by antimicrobial peptides show significant disorder, Biochim. Biophys. Acta 1778 (2008) 2308–2317.
[71] K. Matsuzaki, K. Sugishita, N. Ishibe, M. Ueha, S. Nakata, K. Miyajima, R.M. Epand, Relationship of membrane curvature to the formation of pores by magainin 2, Biochemistry 37 (1998) 11856–11863.
[72] K. Matsuzaki, S. Yoneyama, K. Miyajima, Pore formation and translocation of melittin, Biophys. J. 73 (1997) 831–838.
[73] D.H. Lloyd, Alternatives to conventional antimicrobial drugs: a review of future prospects, Vet. Dermatol. 23 (2012) 299–304, (e259–260).
[74] D. Venugopal, D. Klapper, A.H. Srouji, J.B. Bhonsle, R. Borschel, A. Mueller, A.L. Russell, B.C. Williams, R.P. Hicks, Novel antimicrobial peptides that exhibit activity against select agents and other drug resistant bacteria, Bioorg. Med. Chem. 18 (2010) 5137–5147.
[75] A. Nijnik, R. Hancock, Host defence peptides: antimicrobial and immunomodulatory activity and potential applications for tackling antibiotic-resistant infections, Emerg. Health Threats J. 2 (2009) e1.
[76] K.L. Lam, H. Wang, T.A. Siaw, M.R. Chapman, A.J. Waring, J.T. Kindt, K.Y. Lee, Mechanism of structural transformations induced by antimicrobial peptides in lipid membranes, Biochim. Biophys. Acta 1818 (2012) 194–204.